Defect formation and mechanical stability of perovskites based on LaCrO₃ for solid oxide fuel cells (SOFC)

K. Hilpert*, R.W. Steinbrech, F. Boroomand, E. Wessel, F. Meschke, A. Zuev, O. Teller, H. Nickel, L. Singheiser

Research Center Juelich, Institute for Materials in Energy Systems (IWV-2), 52425 Juelich, Germany

Abstract

Perovskites on the basis of $LaCrO_3$ are of interest as ceramic interconnect materials for the development of solid oxide fuel cells (SOFCs). The interconnects are exposed to oxidising and reducing atmospheres under operating conditions. Oxygen vacancy formation was determined as a function of oxygen partial pressure between 1 and 10^{-22} bar at temperatures between 900 and 1100 °C. Different perovskite compositions made of $(La,Ca/Sr)CrO_{3-\delta}$, $La(Cr,Mg)O_{3-\delta}$, $La(Cr,Mg/Cu/Co,Al)O_{3-\delta}$, and $(La,Ca)(Cr,Al)O_{3-\delta}$ were investigated. Defect models were evaluated to describe the oxygen vacancy formation and the respective thermodynamic data were determined. The results are used to explain existing literature data on the isothermal expansion of $LaCrO_3$ based perovskites under reducing conditions. Complementary mechanical measurements with selected perovskite compositions revealed that lower oxygen partial pressure causes higher stiffness, strength and fracture toughness. The change in properties is discussed in terms of the observed ferroelastic domains and the interaction of the domain wall motion with the oxygen vacancies.
© 2003 Elsevier Ltd. All rights reserved.

Keywords: Defects; Fuel cells; Isothermal expansion; LaCrO₃; Mechanical properties; Perovskites

1. Introduction

Acceptor- and donor-doped lanthanum chromites (e.g. $La_{1-x}M_xCrO_{3-\delta}$ or $LaCr_{1-x}M'_xO_{3-\delta}$) (M = Ca or Sr, M' = Mg) have high melting points, good electrical conductivity, and stability in reducing and oxidizing environments at high temperatures. These properties make the perovskites attractive for use in high temperature SOFCs as ceramic interconnects or as coatings for metallic interconnects at operating temperatures of 800–1000 °C.[1,2] As electrically conducting refractory material they are also of interest for electrode applications in magnetohydrodynamic (MHD) generator channels[3] and as heating elements in high temperature furnaces. Other metals than alkaline earth metals are often added to $La_{1-x}M_xCrO_{3-\delta}$ or $LaCr_{1-x}M_xO_{3-\delta}$ in order to adjust e.g. the thermal expansion or to decrease the sintering temperatures necessary for producing high density components.

The electronic conductivity of the stoichiometric $LaCrO_3$ compound is increased by substituting divalent metal ions on either the A- or B-sites of the ABO_3 lattice.[4] The replacement of a trivalent ion by a divalent ion is electrically compensated by the formation of tetravalent chromium ions at high oxygen partial pressure, where the oxygen vacancy concentration has been found to be close to zero.[5] By annealing in reducing atmosphere the compound loses oxygen, the charge neutrality is maintained by the formation of oxygen vacancies,[5–8] and the electronic conductivity decreases with decreasing pO_2. The change in valence state of the chromium ions and the change of oxygen vacancy concentration in reducing environments leads to volume expansion,[5,9–12] which can result in residual stresses in the interconnects of SOFCs under operating conditions. However, it should be noted that compositional changes allow to suppress at least to a certain extent the volume expansion (e.g. Ref. 12). The annealing of the perovskites in reducing atmosphere may also have influence

---

* Corresponding author. Tel.: +49-2461-613700; fax: +49-2461-613699.

E-mail address: k.hilpert@fz-juelich.de (K. Hilpert).

on their mechanical properties.[13–16] Increasing,[13,14] unaffected[15] and decreasing strength[16] as a function of decreasing oxygen partial pressure have been reported recently.

This paper summarises results obtained in a research project of the Deutsche Forschungsgemeinschaft (DFG) within the priority programme "Multifunctional Materials". The main goal of the work is to provide a better understanding of the structural changes in $LaCrO_3$ base perovskites related with a reduction of oxygen partial pressure. In this respect, also the correlation between defect formation and isothermal volume expansion is elaborated for the compositions shown in Table 1. In addition, the question is addressed, how the structural changes affect the macroscopic mechanical behaviour of the perovskites. Complementary studies with two selected compositions are described, which focus on the stress–strain characteristics and on the fracture toughness.

2. Experimental

2.1. Material and sample preparation

Powders of different substituted lanthanum chromite compositions LCC, LSC20, LCCA, LCCuA, and LCCoA (definition of acronyms cf. Table 1) were synthesised by solid-state reaction from the corresponding nitrates. The desired compositions were prepared by dissolving known amounts of the selected nitrates in water. The homogeneous powder mixtures were dried at 200 °C and then calcined in air at 800 °C for 2 h and heated to 1300 °C for 12 h. For all compositions, X-ray diffraction analysis revealed no second phase. The powders were pressed into pellets and sintered at 1500 °C for 1 h. The chemical composition after sintering was confirmed by chemical analysis (ICP-OES) within the analytical error of ±3%. The phase composition was checked by X ray diffraction, XRD.

The LSCV and LCMA perovskites (cf. Table 1) were obtained as slabs and discs with high density. Riso National Laboratory, Denmark, provided LSCV and H. Bausinger, Dornier, Friedrichshafen, Germany, the LCMA variant. For details with respect to the LCMA source see Ref. 12. Micrographs of both perovskite variants are shown in Fig. 1, as obtained by atomic force microscopy. The high density of the materials was

achieved by sintering at 1800 or 1900 K for dwell times between 2 and 5 h. Other LCC and LSC variants were supplied by Seattle Speciality Ceramics, Inc., USA (Praxair) as plates with low density (about 65% of the theoretical density).

The slabs were cut into bars ($2/3 \times 4 \times 45$ mm^3, LSCV) and discs (diameter 22 mm, thickness 0.4 mm, LCMA) for the measurement of the stress–strain behaviour. Toughness was only determined with thick (4 mm) notched bend bars. Thus in addition to the bulk LSCV samples, laminated LCMA bars ($3 \times 4 \times 45$ mm^3) were prepared. The samples were V-notched to conduct Single Edge V-Notch Bending tests (SEVNB[17]). With a 200 μm diamond saw blade, first pre-notches were machined to a depth of about 25% of the sample height. Using a diamond suspension and a razor blade, the pre-notch was then extended and sharpened to a final depth of about 40% of the sample height.

Different amounts of oxygen vacancies were adjusted by annealing the samples at 1273 K for 100 h in an Ar/H$_2$ atmosphere and cooling down to room temperature over a time period of 60 s. By this moderate quenching procedure it was possible to freeze oxygen vacancies in the sample material without noticeable formation of thermal shock microcracks. To exclude pure temperature effects, the atmospheric reference samples were given the same heat treatment in air. Composition and material integrity were checked by determination of the unit cell volume (XRD) and by dye-penetration tests in combination with optical microscopy, respectively.

2.2. Defect formation and isothermal expansion

The formation of oxygen vacancies at elevated temperatures was studied by isothermal thermogravimetry as a function of oxygen partial pressure at different temperatures between 900 and 1100 °C. The weight change of a given composition was measured with a thermo-balance system (Fig. 2). Cylindrical samples of the compositions listed in Table 1 with a weight between 1500 and 2500 mg were used for the thermogravimetric measurements. The weight change was measured to an accuracy of ±0.1 μg with a Mettler UMT5 balance. Different oxygen partial pressures were adjusted and maintained by using the H$_2$/H$_2$O/Ar system with flow rates of about 30 ml/min and fixed by means of an electrochemical pump which was also used as an oxygen

Table 1
Sample compositions and labels

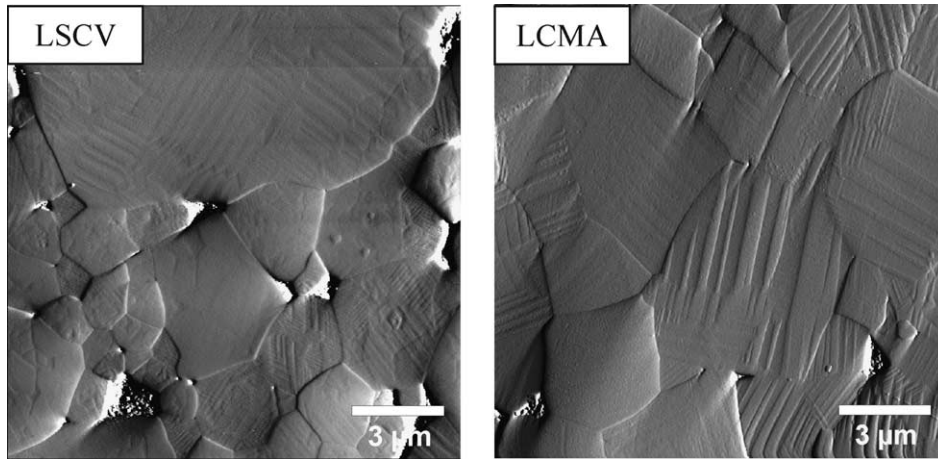| Doped on A site	Label	Doped on A site and B site	Label	Doped on B site	Label
$La_{0.90}Ca_{0.10}CrO_{3-\delta}$	LCC10	$La_{0.80}Sr_{0.20}Cr_{0.97}V_{0.03}O_{3-\delta}$	LSCV	$LaCr_{0.79}Mg_{0.05}Al_{0.16}O_{3-\delta}$	LCMA
$La_{0.80}Ca_{0.20}CrO_{3-\delta}$	LCC20	$La_{0.95}Ca_{0.05}Cr_{0.84}Al_{0.16}O_{3-\delta}$	LCCA	$LaCr_{0.79}Cu_{0.05}Al_{0.16}O_{3-\delta}$	LCCuA
$La_{0.80}Sr_{0.20}CrO_{3-\delta}$	LSC20			$LaCr_{0.79}Co_{0.05}Al_{0.16}O_{3-\delta}$	LCCoA

Fig. 1. AFM micrographs of (a) LSCV and (b) LCMA. Both perovskites have large matrix grains, which show surface traces of ferroelastic domain switching. LCMA contains significantly less second phase pockets.
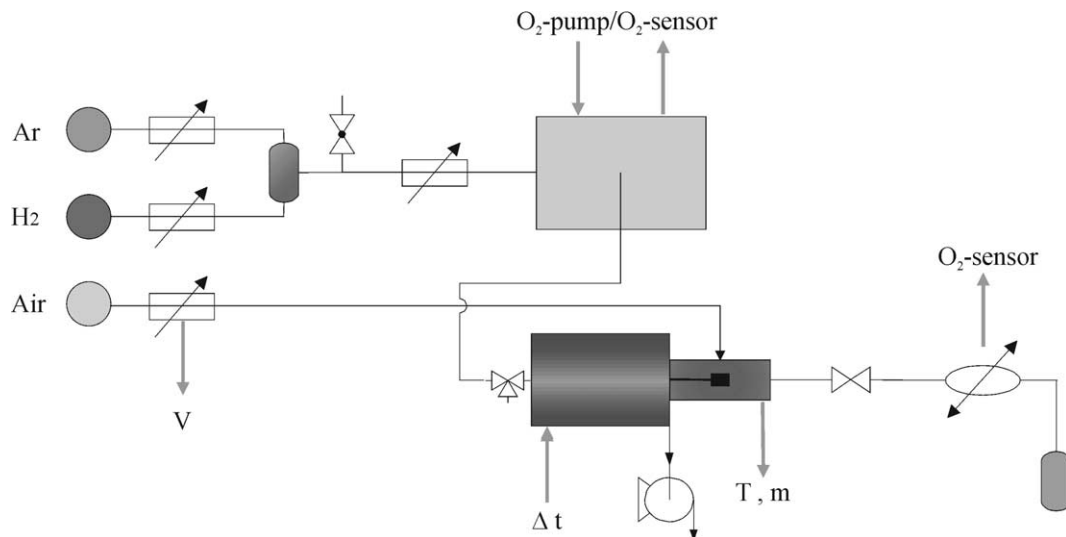

Fig. 2. Experimental setup developed for isothermal gravimetric measurement of oxygen vacancy formation consisting of thermobalance, gas mixing system, oxygen pump/oxygen sensor upstream, and oxygen sensor downstream.

sensor. The pump/sensor was arranged downstream before the balance. The pO_2 was additionally monitored by passing the exit gases through a calibrated oxygen sensor. Each sample was heated to the measurement temperature in an oxidizing atmosphere and allowed to equilibrate before stepwise change of pO_2.

The measurements of isothermal volume expansion were performed by H. Bausinger[12] using a Netzsch 402C dilatometer and $25 \times 4 \times 1$ mm^3 bars. The samples were equilibrated at 1000 °C in argon. The oxygen partial pressure was then decreased in steps from 10^{-11} to 10^{-19} bar and the sequence was retraced again to oxidising conditions.

2.3. Mechanical tests

The fracture stress of the LSCV bars was measured in 4-point bending fixture in which the distance between inner and outer load lines were 20 and 40 mm, respectively. For the thinner LCMA discs a ring on ring loading device with rings of 9.4 and 4.7 mm diameter was used. In both testing geometries the central displacement during bending was recorded using a LVDT system. The experimentally determined load-displacement curves were converted into stress–strain curves applying well established linear elastic relationships (DIN 51110 and DIN 52292/1).

The toughness determination was conducted with the SEVNB testing technique.[17] The samples were loaded under conditions of controlled crack growth in 4-point bending. The crack growth was observed in-situ with a long distance microscope (Questar QM 100). With the corresponding data for load, deflection and crack length the stress intensity[18] was calculated and balanced with the fracture toughness.

3. Results

3.1. Defect formation

Figs. 3–6 show the results of the thermogravimetric measurements on the defect formation for a temperature of 1000 °C. The weight change caused by the vacancy formation and the total weight of the sample investigated were used to compute the oxygen nonstoichiometry of the different perovskites. Stoichiometric composition was assumed for all perovskites investigated in this work except LCCuA if an atmosphere of air with a pressure of 1 bar is present. For stoichiometric composition ($\delta = 0$) the relation $\partial \delta / \partial \log(p_{O_2}) = 0$ is valid under these conditions. In an

analogous way, stoichiometric composition ($\delta = 0$) for LCCuA was assumed to be present at an oxygen partial pressure of 1 bar (cf. Fig. 6). The loss of oxygen observed for the different materials is described by the defect equilibria listed in Table 2 using the Kröger–Vink notation. The equilibrium constants of these reactions are used to obtain model relations describing the measurement results shown in Figs. 3–6. The measurement points in these figures are fitted well by these equations yielding the equilibrium constant of the reactions shown in Table 2. The full lines shown in these figures result from the fitting, the respective equilibrium constants are listed in Table 2. Details of the defect models and the fitting procedure are reported in Refs. 19–21
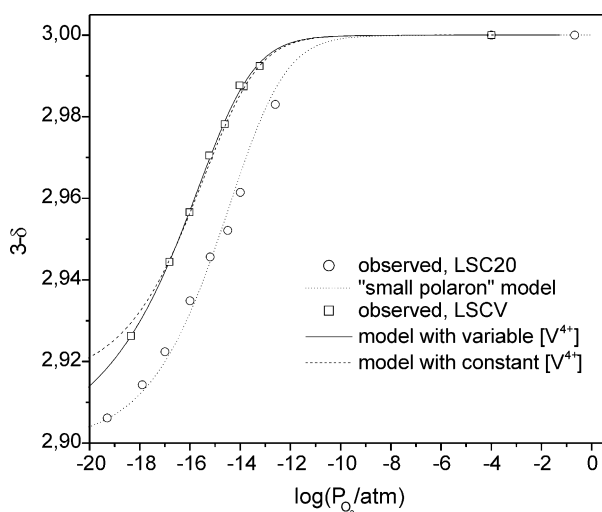

Fig. 3. Nonstoichiometry of La$_{0.80}$Sr$_{0.20}$CrO$_{3-\delta}$ (LSC20) and La$_{0.80}$Sr$_{0.20}$Cr$_{0.97}$V$_{0.03}$O$_{3-\delta}$ (LSCV) at 1000 °C. Fitted curves result on the basis of defect models (see text).
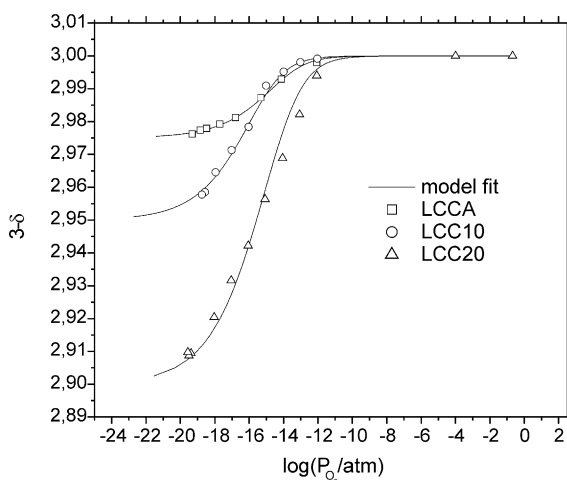

Fig. 5. Nonstoichiometry of LaCr$_{0.79}$Co$_{0.05}$Al$_{0.16}$O$_{3-\delta}$ (LCCoA), La$_{0.95}$Ca$_{0.05}$Cr$_{0.84}$Al$_{0.16}$O$_{3-\delta}$ (LCCA), and LaCr$_{0.79}$Mg$_{0.05}$Al$_{0.16}$O$_{3-\delta}$ (LCMA) at 1000 °C. Fitted curves result on the basis of defect models (see text).

Fig. 4. Nonstoichiometry of La$_{0.95}$Ca$_{0.05}$Cr$_{0.84}$Al$_{0.16}$O$_{3-\delta}$ (LCCA), La$_{0.90}$Ca$_{0.10}$CrO$_{3-\delta}$ (LCC10), and La$_{0.80}$Ca$_{0.20}$CrO$_{3-\delta}$ (LCC20) at 1000 °C. Fitted curves result on the basis of defect models (see text).
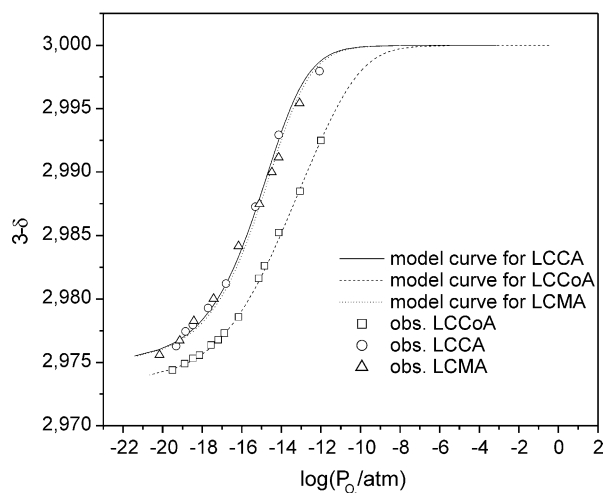

Fig. 6. Nonstoichiometry of LaCr$_{0.79}$Co$_{0.05}$Al$_{0.16}$O$_{3-\delta}$ (LCCoA) and LaCr$_{0.79}$Cu$_{0.05}$Al$_{0.16}$O$_{3-\delta}$ (LCCuA) at 1000 °C. Fitted curves results on the basis of defect models (see text).

Table 2
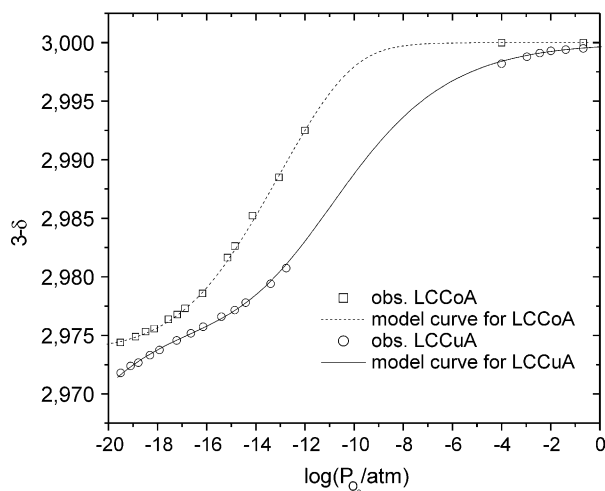Temperature range of measurements of oxygen vacancy formation as well as reactions of defect formation together with their thermodynamic properties (equilibrium constant K^0, enthalpy change, ΔH^0, and entropy change, ΔS^0) for different perovskite compositions

Composition (cf. Table 1)	Temperature range, K	Reaction	K^0 at 1273 K, and reference	ΔH^0, kJ/mol	ΔS^0, J/(K*mol)
LCC10	1173–1373	$O_O^\times + 2Cr_{Cr}^\bullet \Longleftrightarrow V_O^{\bullet\bullet} + 1/2 O_2(g) + 2Cr_{Cr}^\times$	1.63×10^{-8} [19]	301.2 [19]	86.4 [19]
LCC20	1273	$O_O^\times + 2Cr_{Cr}^\bullet \Longleftrightarrow V_O^{\bullet\bullet} + 1/2 O_2(g) + 2Cr_{Cr}^\times$	2.58×10^{-8} [19]	–	–
LCCA	1173–1373	$O_O^\times + 2Cr_{Cr}^\bullet \Longleftrightarrow V_O^{\bullet\bullet} + 1/2 O_2(g) + 2Cr_{Cr}^\times$	1.13×10^{-7} [21]	232.2	49.4
LCMA	1173–1373	$O_O^\times + 2Cr_{Cr}^\bullet \Longleftrightarrow V_O^{\bullet\bullet} + 1/2 O_2(g) + 2Cr_{Cr}^\times$	1.55×10^{-7} [20]	241.3	58.9
LSC20	1173–1373	$O_O^\times + 2Cr_{Cr}^\bullet \Longleftrightarrow V_O^{\bullet\bullet} + 1/2 O_2(g) + 2Cr_{Cr}^\times$	4.99×10^{-8} [21]	–	–
LSCV	1173–1373	$O_O^\times + 2Cr_{Cr}^\bullet \Longleftrightarrow V_O^{\bullet\bullet} + 1/2 O_2(g) + 2Cr_{Cr}^\times$	1.45×10^{-8} [21]	388	155
		$O_O^\times + 2V_{Cr}^\bullet \Longleftrightarrow V_O^{\bullet\bullet} + 1/2 O_2(g) + 2V_{Cr}^\times$	3.48×10^{-12} [21]	–	–
		$Cr_{Cr}^\times + V_{Cr}^\bullet \Longleftrightarrow Cr_{Cr}^\bullet + V_{Cr}^\times$	1.55×10^{-2} [21]	–	–
LCCoA	1173–1273	$O_O^\times + 2Cr_{Cr}^\bullet \Longleftrightarrow V_O^{\bullet\bullet} + 1/2 O_2(g) + 2Cr_{Cr}^\times$	3×10^{-5} [21]	225.6	90
		$O_O^\times + 2Co_{Cr}^\times \Longleftrightarrow V_O^{\bullet\bullet} + 1/2 O_2(g) + 2Co_{Cr}^/$	1.2×10^{-9} [21]	220.3	13
		$Cr_{Cr}^\bullet + Co_{Cr}^\times \Longleftrightarrow Cr_{Cr}^\times + Co_{Cr}^/$	6.01×10^{-3} [21]	3.5	−38
LCCuA	1273	$O_O^\times + 2Cu_{Cr}^\times \Longleftrightarrow V_O^{\bullet\bullet} + 1/2 O_2(g) + 2Cu_{Cr}^/$	2.47×10^{-8}	–	–
		$O_O^\times + 2Cu_{Cr}^\bullet \Longleftrightarrow V_O^{\bullet\bullet} + 1/2 O_2(g) + 2Cu_{Cr}^{//}$	4.69×10^{-14}	–	–

Measurements at 900 and 1100 °C as well as at 900 and 950 °C (for LCCoA) were carried out in addition to those at 1000 °C for some of the perovskite materials listed in Table 1. Equilibrium constants are evaluated in the same way as described for 1000 °C. The temperature dependence of the equilibrium constant is given as

$$K = \exp\left(-\frac{\Delta G^\circ}{RT}\right) = \exp\left(\frac{\Delta S^\circ}{R}\right)\cdot\exp\left(-\frac{\Delta H^\circ}{RT}\right)$$

where ΔG°, ΔH° and ΔS° are the changes of the Gibbs energy, the enthalpy, and the entropy, respectively, of the reactions considered. The values of ΔH° and ΔS°, therefore, result from the slope and the intercept, respectively, of the plot $\ln(K)$ vs. $1/T$ and are given in Table 2.
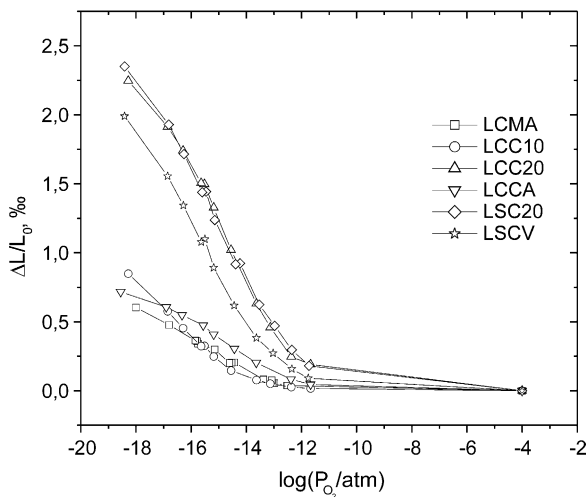

Fig. 7. Linear isothermal expansion as function of the oxygen partial pressure p(O$_2$) for different perovskite compositions (cf. Table 1) at 1000 °C.

3.2. Swelling

At oxygen partial pressures below pO$_2\approx10^{-12}$ bar the swelling effect of the doped lanthanum chromites becomes noticeable (Fig. 7[12,20]) and develops different slopes for different compositions. At pO$_2\approx10^{-18}$ a factor 3 lower swelling values are measured for LCMA compared to the other extreme of the investigated perovskites, LSC20, which expands by $\Delta L/L\approx0.23\%$.

3.3. Stress–strain behaviour

The stress–strain curves of LSCV and LCMA show a pseudo-plastic deformation behaviour (Fig. 8), which is more pronounced in the case of LSCV. In general, the samples which are heat-treated in air, exhibit the strongest non-linearity. The onset of non-linear deformation shifts to higher stress with decreasing pO$_2$.

The stress–strain curves of both perovskites also reveal an increase of stiffness (elastic modulus) with decreasing oxygen partial pressure. The stiffness of LCMA nearly triples when pO$_2$ is reduced from atmosphere to 10^{-20} bar. LSCV shows a similar behaviour, but appears more compliant for all investigated oxygen partial pressure levels.

Similar trends are observed for the fracture stress (Fig. 9). Despite considerable scatter and the limited amount of experimental data, an increase of bending strength with decreasing oxygen partial pressure can be deduced.

3.4. Fracture behaviour

Both perovskites exhibit a rising fracture toughness with crack extension (K_R-curve behaviour, Fig. 10). After annealing in air, the K_R-curve of the LSCV mate-
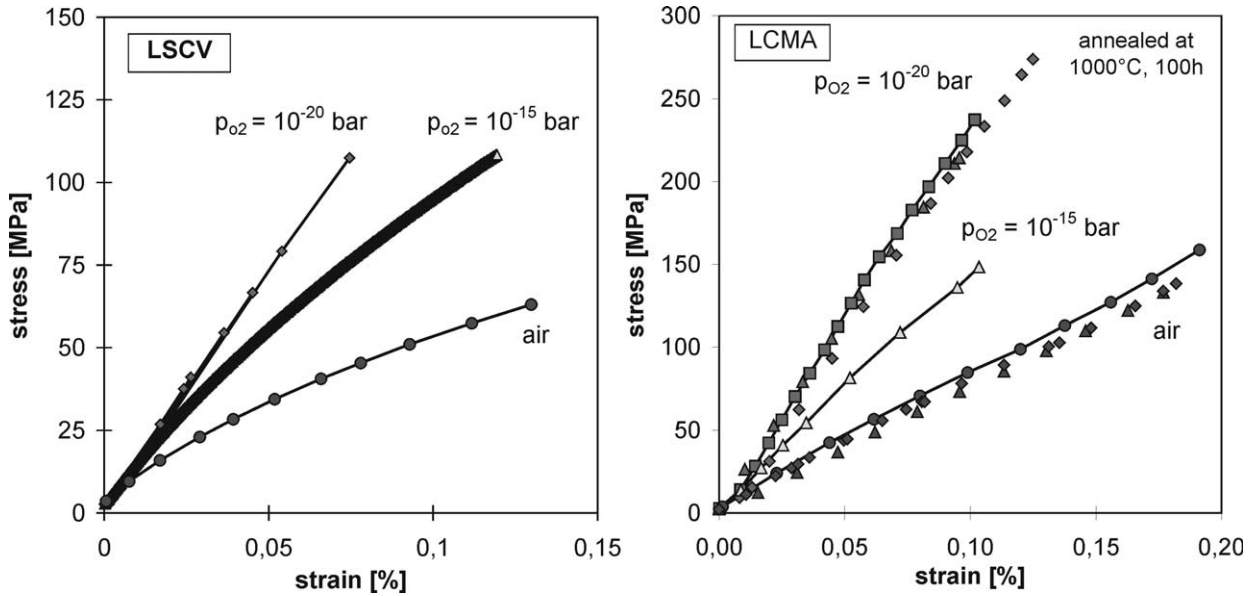
Fig. 8. Stress–strain curves of LSCV and LCMA measured at room temperature after previous heat treatment at 1000 °C/100 h with different oxygen partial pressures.

rial starts with an initial value of 1.1 MPa√m and increases to 1.4 MPa√m after a crack extension of 500 µm. The curve tends to saturate in a plateau value of about 1.6 MPa√m. LCMA exhibits significantly higher toughness values. The respective K_R-curve starts with an initial value of 1.4 MPa√m and increases to 2.1 MPa√m after a crack extension of 500 µm.

Decreasing pO₂ causes a shift of the fracture toughness curve of both materials to higher values without a significant change in slope. After annealing at pO₂ = 10⁻¹⁵

bar the K_R-curve of the LSCV perovskite reaches a level, which is about 0.5 MPa√m higher than that in air.

Similarly, the initial toughness value of the LCMA material rises from 1.5 to a maximum of 2.3 MPa√m. This value corresponds to an increase of about 60%. However, compared to monolithic ceramics[22] the K_R-curves of both perovskites are less pronounced, and it can be assumed that the initial fracture toughness values practically determine the fracture stress observed in the strength tests.
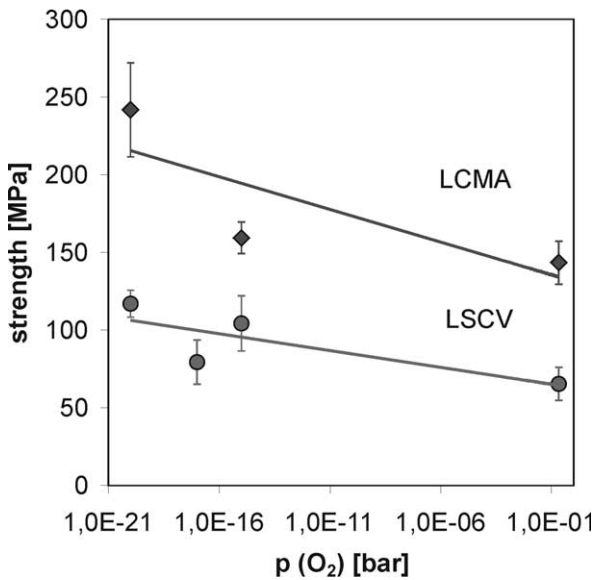

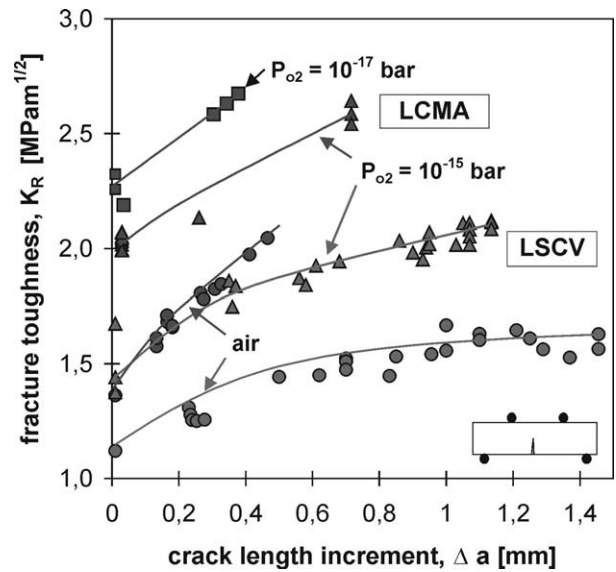Fig. 9. Fracture stress as a function of oxygen partial pressure. (Data from Fig. 8).

Fig. 10. Fracture toughness curves of LSCV and LCMA. Lower oxygen partial pressure increases toughness values in both perovskites.

4. Discussion

4.1. Oxygen vacancy formation and defect structure

Figs. 3–6 show that the experimental results obtained are excellently represented by the selected defect models (see Table 2). The chromite compositions investigated can be divided into two different groups according to the nature of the dopants.

The first group consists of the compositions which contain the alkaline earth metal Ca, Sr or Mg as a dopant. The characteristic defect structure of such chromites is that tetravalent chromium is formed under oxidizing conditions as a result of charge compensation due to acceptor doping in accordance with the Verwey principle.[23] The process of oxygen release from the chromite lattice under reducing conditions is, therefore, accompanied by the transition of Cr^{4+} to Cr^{3+} according to the "small polaron" reaction (Table 2). There is a general trend for this group that the vacancy concentration at low oxygen potential increases if the content of the alkaline earth metals is raised as shown in Fig. 4. It is interesting to note that the results obtained for LCMA containing 5% Mg on B site and those of LCCA containing the same amount of Ca agree with each other in practical terms (Fig. 5). In contrast to this, the result obtained for LSC20 and LSCV deviate from each other significantly although these chromites have the same Sr content on A sites. This can be explained by the influence of the vanadium on B site in LSCV. Vanadium seems to accept the 4+ state of oxidation easier as compared to Cr thereby compensating in part the negative charge induced by the Sr^{2+} presence on A site (3% of the Sr content). This means LSCV shows the same behavior as $La_{0.83}Sr_{0.17}CrO_{3-\delta}$ at high and intermediate oxygen partial pressures as it is demonstrated in Fig. 2 by the comparatively good agreement between the measurement results and the "small polaron" model using a reduced Sr content. However, the results shown in Fig. 2 are in favor of the selected defect model which allows also the reduction $V^{4+} \rightarrow V^{3+}$. This reduction seems to start at very low oxygen partial pressures.

The Co- and Cu-doped chromites, LCCoA and LCCuA, form the second group of chromites. Unlike the compounds from the first group, the second group does not contain alkaline earth metals which could provide Cr^{4+} cations as a result of charge compensation in accordance with the Verwey principle. However, the existence of tetravalent charge carriers follows from the results of electrical conductivity and thermopower measurements for $LaCr_{1-x}Co_xO_3$.[24] This means that some amount of the Cr^{4+} cations can be produced by the reaction $Cr^{3+} + Co^{3+} = Cr^{4+} + Co^{2+}$ similar to Jonker's proposal for $La(Mn,Co)O_3$.[26] The fit results shown in Fig. 5 confirm this assumption. Moreover, the site occupancy for LCCoA at 1273 K calculated in air by the use of the equilibrium constants listed in Table 2 shows good agreement with that from thermopower measurements.[24] The results mentioned above for Co-doped chromites allow the conclusion that the loss of oxygen in reducing environment is accompanied by both $Cr^{4+} \rightarrow Cr^{3+}$ and $Co^{3+} \rightarrow Co^{2+}$ transitions.

The defect structure of the Cu-doped chromite LCCuA differs significantly from that of the other compositions investigated (Table 2). Two particularities have to be highlighted in this respect. Firstly, LCCuA remains slightly understoichiometric with respect to oxygen at 1273 K in air. The second particularity consists in the lack of the change of the Cr^{3+} oxidation state over the complete oxygen partial pressure range investigated (see Table 2). In contrast to this, copper changes its oxidation state continuously from 3+ via 2+ to 1+ if the oxygen partial pressure decreases. The reactions for the formation of oxygen vacancies in LCCuA shown in Table 2 proceed simultaneously. The first point of inflection of the curve shown in Fig. 6 at an oxygen partial pressure $pO_2 = 10^{-11}$ atm corresponds to equal concentrations of Cu^{3+} and Cu^{2+}. The second point of inflection is observed at $p(O_2) = 10^{-17}$ atm when the concentration of the Cu^{3+} becomes equal to that of Cu^{1+} and, therefore, the concentration of the Cu^{2+} starts to decrease if the oxygen partial pressure is further diminished.

4.2. Correlation between defect structure and isothermal expansion

The isothermal expansion determined as a function of the oxygen partial pressure at 1000 °C for different chromite compositions and reported in Refs. 12 and 19 is used in the present study to determine the correlation between the isothermal expansion and the defect structure described in Section 4.1. The formation of oxygen vacancies at low oxygen partial pressures is accompanied by the reduction of Cr^{4+} to Cr^{3+} for all chromites of the first group defined in Section 4.1. For this reason, there are two possible mechanisms according to which the observed isothermal expansion can be explained. The first mechanism is a dimensional one, which consists in the increase of the mean size of the chromium cations due to the substitution of large Cr^{3+} for small Cr^{4+} by the reduction. The second mechanism is the coulomb repulsion between Cr cations because of the oxygen vacancy formation.[11] In order to reveal which of the mechanisms mentioned above contributes most to the lattice expansion the average size of the B site cations is plotted versus the oxygen partial pressure. The respective changes in radii (Fig. 11) were computed by taking into account the ionic radii of the B site cations[26] and their concentration which was determined on the basis of the defect structure evaluated for the different chromite compositions (see Section 3.1). The
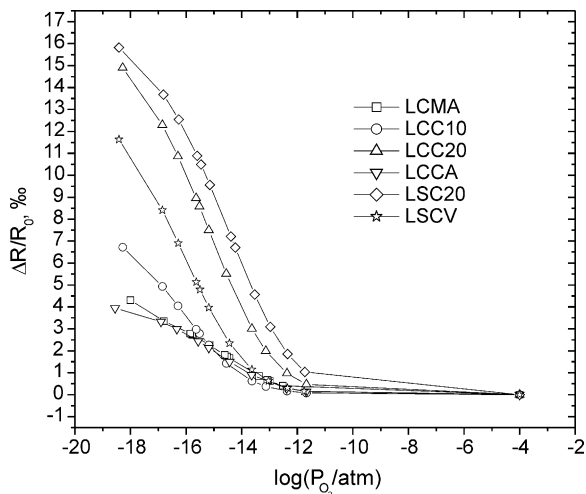
Fig. 11. Relative change of the average radius of the B site cations as function of the oxygen partial pressure p(O₂) for different perovskite compositions (cf. Table 1).

Fig. 13. Linear isothermal expansion as function of the oxygen non-stoichiometry δ for different perovskite compositions (cf. Table 1) at 1000 °C.
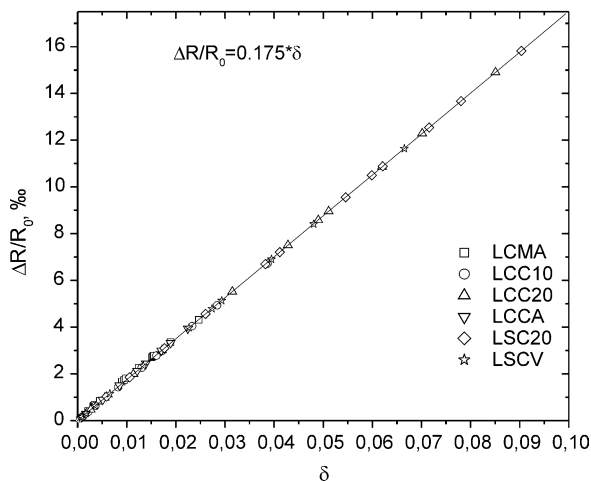

Fig. 12. Relative change of the average radius of the B site cations as function of the oxygen nonstoichiometry δ for different perovskite compositions (cf. Table 1).

Fig. 14. Linear isothermal expansion as function of the relative change of the average radius of the B site cations for different perovskite compositions (cf. Table 1) at 1000 °C.

crystal ionic radii (19) accepted for the B site cations in octahedral coordination ($CN = 6$) are $r_{Cr}^{3+} = 0.755$ Å, $r_{Cr}^{4+} = 0.69$ Å, $r_{V}^{3+} = 0.78$ Å, and $r_{V}^{4+} = 0.72$ Å. Crystal radii are employed in this paper, instead of effective ionic radii used in our previous paper,[21] because of their close correspondence to the physical size of ions in solids.[21] The comparison of Figs. 7 and 11 reveals that the trend in the expansion behavior (Fig. 7) and the trend in the change of average radius of the B site cations (Fig. 11) are similar. The isothermal expansion and the change of average radius of the B site cations increase at constant oxygen partial pressure if the alkaline earth metal content is raised. On other hand, if the chromites contain the same amount of a dopant, such as in LCMA and LCCA, they have about the same expansion and average change in radius under similar conditions, indifferently whether the dopant is on A or B site.
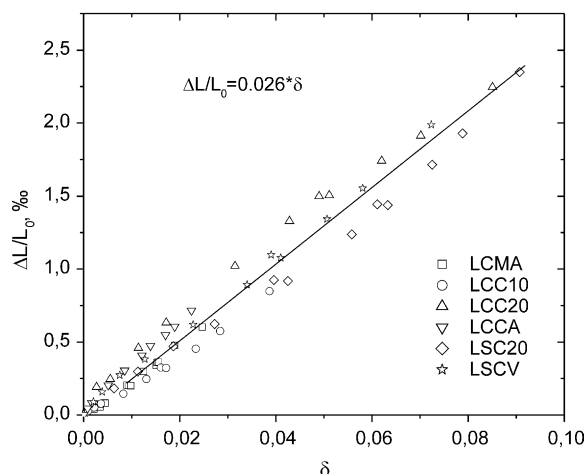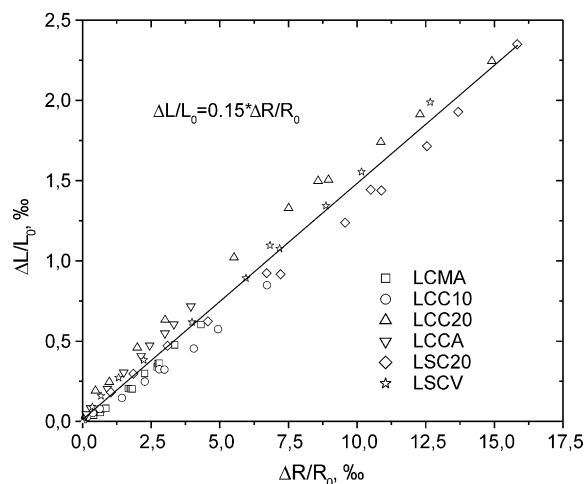
According to the simple defect model accepted for compounds with an alkaline earth metal as dopant the decrease of the Cr^{4+} content at the same oxygen vacancy concentration is independent of the nature, lattice site, and concentration of the dopant. The change of the average radius of the B site cations for such chromites, therefore, agrees well at the same value of oxygen nonstoichiometry (Fig. 12). Moreover, this figure shows a strong linear dependence of the change of the average radius from the oxygen nonstoichiometry. A similar relation has to be expected between the isothermal expansion and the oxygen vacancy concentration if the change of the average B site cation radius contributes most to the isothermal expansion. Fig. 13
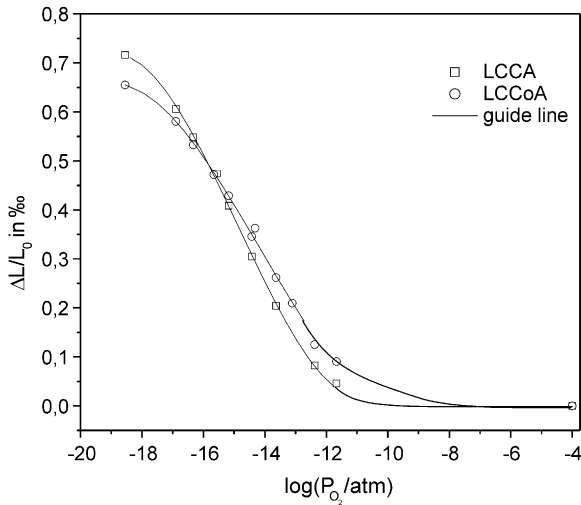
Fig. 15. Linear isothermal expansion as function of the oxygen partial pressure $p(O_2)$ for $La_{0.95}Ca_{0.05}Cr_{0.84}Al_{0.16}O_{3-\delta}$ (LCCA) and $LaCr_{0.79}Co_{0.05}Al_{0.16}O_{3-\delta}$ (LCCoA) at 1000 °C.
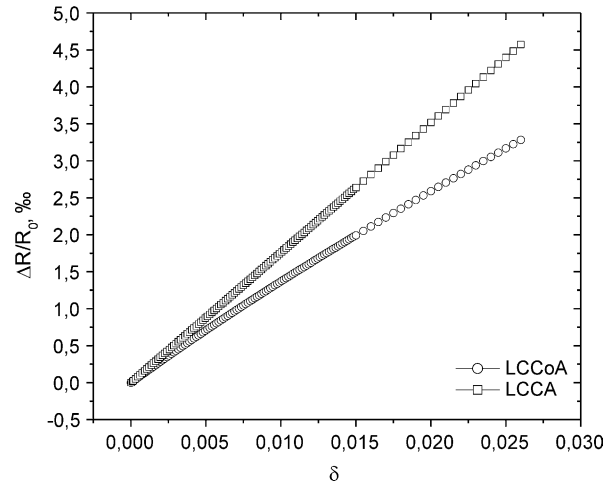

Fig. 17. Relative change of the average radius of the B site cations as function of the oxygen partial pressure for $LaCr_{0.79}Co_{0.05}Al_{0.16}O_{3-\delta}$ (LCCoA) and $La_{0.95}Ca_{0.05}Cr_{0.84}Al_{0.16}O_{3-\delta}$ (LCCA) at 1000 °C.
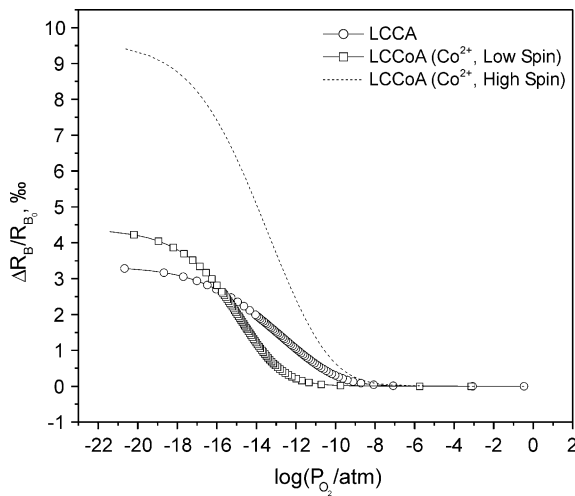

Fig. 16. Relative change of the average radius of the B site cations as function of the oxygen partial pressure $p(O_2)$ for $La_{0.95}Ca_{0.05}Cr_{0.84}Al_{0.16}O_{3-\delta}$ (LCCA) and $LaCr_{0.79}Co_{0.05}Al_{0.16}O_{3-\delta}$ (LCCoA) for different spin states at 100 °C.
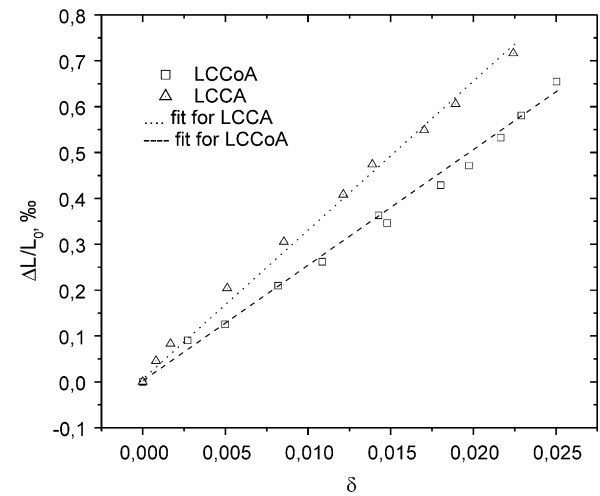

Fig. 18. Linear isothermal expansion as function of the oxygen nonstoichiometry δ for $La_{0.95}Ca_{0.05}Cr_{0.84}Al_{0.16}O_{3-\delta}$ (LCCA) and $LaCr_{0.79}Co_{0.05}Al_{0.16}O_{3-\delta}$ (LCCoA) at 1000 °C.

shows the isothermal expansion plotted for all alkaline earth metal doped chromites versus the oxygen non-stoichiometry. The figure reveals that in spite of the scatter which may be caused by experimental errors there is a linear trend in the expansion as function of the oxygen non-stoichiometry. The relation $\Delta L/L_0 = 0.15(\Delta R/R_0)$ can be used to predict the isothermal expansion as it is shown by Fig. 14.

The substitution of Co or Cu for Cr in lanthanum chromite instead of an alkaline-earth metal as a dopant leads to a significant change of the defect structure (cf. Section 3.1). These chromites should, therefore, show an isothermal expansion behavior different from that of chromites doped with an alkaline earth metal.

Isothermal expansion of LCCoA was determined for an oxygen partial pressure which covers also the conditions of a fully occupied oxygen sublattice.[12] This is not the case for LCCuA which shows significant oxygen vacancy formation at $p(O_2) = 10^{-4}$ bar (Fig. 6) the highest oxygen partial pressure adjusted in the isothermal expansion measurements. The correlation between the oxygen vacancy formation and the isothermal expansion is, therefore, only considered for LCCoA. The isothermal expansion is compared with

that of LCCA due to the similar composition (5% dopant) of LCCA and LCCoA. Figs. 15 and 16 show the oxygen partial pressure dependences of the isothermal expansion and the computed relative change of the average radius of the B-site ions, respectively, for LCCoA and LCCA. The calculated change of the B-site ionic radii is based on the concentrations of different species and their effective ionic radii.[26] The radii for Co^{2+} and Co^{3+} were adopted in octahedral coordination ($CN = 6$) as: $r_{Co}^{3+} = 0.75$ Å (HS), $r_{Co}^{2+} = 0.79$ Å (LS) and $r_{Co}^{2+} = 0.885$ Å (HS), where LS and HS correspond to low and high spin state, respectively. Fig. 16 shows the results for the two spin states, since it was not known whether Co^{2+} exists in low or in high spin state. Fig. 16 may indicate that the presence of the Co^{2+} high spin state is doubtful for LCCoA because the relative change of the average radius of the B-site ions for this state is twice as large than the one calculated for the Co^{2+} low spin state. A Co^{2+} high spin state would lead to an expansion significantly higher than the dependence shown in Fig. 16. The trends in the expansion curves are in good agreement with those of the average radius of the B-site ions for both compounds, if the computation of the change of the average radius is based on the presence of the Co^{2+} low spin state. Not only are the expansion onsets and the onsets of the change of the B-site ionic average radius consistent with each other for the Co^{2+} low spin state, but also the intersections of the expansion and radius change curves are observed at about the same oxygen partial pressure ($\log(p_{O_2}/atm) = -16$). The change of average radius of the B-site ions and the isothermal expansion plotted versus the oxygen nonstoichiometry for both LCCA and LCCoA are shown in Figs. 17 and 18, respectively. The comparison of these figures reveals that the trends in the diagrams are obviously consistent with each other. The consistencies mentioned above indicate that the expansion observed in the (La, Ca)(Cr, Co, Al)O$_3$ system is mainly determined by the relative change of the average B-site ionic radius as it was observed for the other chromite systems mentioned above.

4.3. Mechanical behaviour

Both mechanically tested perovskites, LSCV and LCMA, belong to the first group of chromites with additions of alkaline earth metals. They also show similarities in their mechanical behaviour. The formation of oxygen vacancies by annealing in reducing atmospheres diminishes the pseudo-plasticity, increases the stiffness, and improves the strength and fracture toughness of the two perovskites.

These findings are supported in part by the few investigations on this subject reported in literature. Most of the mechanical tests with ABO$_3$-type perovskites focus on strength as a function of oxygen partial pressure. Gut[13] determined for the same LSCV

material a similar increase of strength. Milleken et al.[14] report an increase (50%) for La$_{0.83}$Sr$_{0.16}$CrO$_3$. However, using similar compositions, Montross et al.[15] observed no improvement in strength. On the other hand, Paulik et al.[16] report a significant decrease in bending strength when testing La$_{0.85}$Sr$_{0.15}$CrO$_3$ and La$_{0.70}$Sr$_{0.30}$CrO$_3$ in hydrogen. A solution of these obvious differences requires not only information about the oxygen vacancy concentration but also detailed knowledge of the microstructural peculiarities of each material. In particular, all microstructural changes that occur with decreasing oxygen partial pressure are of interest, i.e. it is important to know whether phases, grain boundaries, mode of micro-cracking and the failure inducing crack geometry remain unchanged. Although such a detailed analysis was out of the scope of the present work, a common microstructural deformation mechanism was observed in the case of LSCV and LCMA, which allows to explain at least qualitatively the obtained mechanical results.

The AFM micrographs of Fig. 1 show that both perovskites exhibit in some of the grains surface steps caused by domain switching effects. It is suggested that this effect provides the origin of the pseudo-plasticity observed in the stress–strain plots of Fig. 8. Note that a similar stress–strain behaviour is known for perovskites like BaTiO$_3$ and PZT under bending and compression loading,[27,28] where ferroelastic domain switching has been verified as the underlying deformation mechanism. Given the domain switching effect exists in LSCV and LCMA, it is further suggested that the presence of oxygen vacancies affects the motion of the domain walls. Since the onset of non-linear deformation shifts in both perovskites to higher stress with decreasing pO_2 the motion of the domain walls seems increasingly hindered by the growing number of vacancies.

The reason for the increasing stiffness with decreasing pO_2 is still unknown, but could be due to oxygen-vacancy related differences in crystallographic bonding properties.[29] This should influence the resistance to fracture (toughness) and the strength, too. Interestingly a stress-dependent ferroelastic domain switching can also contribute to the observed moderate K_R-curve behaviour of LSCV and LCMA. A rising toughness curve has been reported for ferroelectric perovskites like BaTiO$_3$.[30] In these materials the crack tip stresses induce ferroelastic domain switching and thus generate a process zone, which causes crack tip shielding. It is suggested, but needs further experimental evidence, that the same toughening mechanism is operating in the electrically conductive LaCrO$_3$ perovskites.

Although promising first results are presented here, further microstructural studies are necessary to proove unambiguously the suggested interaction between the

structural defects and the domain wall motion in $LaCrO_3$ variants. Convincing experimental evidence would then also justify efforts to establish a quantitative correlation with the concentration of oxygen vacancies.

5. Conclusions

Oxygen vacancy formation in nine $LaCrO_3$ base perovskites of different composition (Table 1) was determined and correlated with data on the isothermal expansion. Thermomechanical measurements on selected compositions revealed the influence of oxygen vacancies on the mechanical properties.

Defect models were developed which describe the oxygen vacancy formation in the different perovskites. Enthalpy and entropy changes were evaluated for the reactions of the defect formation. The perovskites investigated can be divided into two groups. The chromites containing Ca, Sr or Mg (first group) essentially release oxygen by the transition Cr^{+4} to Cr^{+3} according to the "small polaron" reaction. The composition LSCV may additionally show the transition V^{+4} to V^{+3} at very low oxygen partial pressures. The chromites with no addition of alkaline earth metals but Co or Cu (second group) lead to significant changes in the defect structures since Co and especially Cu tend to reduce their oxidation state. The results obtained on oxygen non-stoichiometry of doped chromite compositions showed the large impact of the nature of the dopants on the defect structure of these chromites.

The correlation between the oxygen non-stoichiometry and the isothermal expansion reveals that the latter can be understood by the change of the average B site cation radius of the perovskites which is obtained from the defect structure.

The complementary thermomechanical measurements with LSCV and LCMA perovskites demonstrated that the stiffness, strength and toughness increase with decreasing oxygen partial pressure. The stress–strain behaviour was qualitatively explained by considering the observed ferroelastic domain structures and by assuming the hindrance of wall motion by the oxygen vacancies.

Under mechanical aspects the LCMA perovskite proved to be advantageous compared to LSCV. LCMA is stiffer and has the higher fracture toughness and strength, which in combination with the lower swelling favours the use of this variant in SOFC stacks.

Acknowledgements

References

1. Minh, N. Q., Ceramic fuel cells. *J. Am. Ceram. Soc.*, 1993, **76**, 563–588.
2. Ruckdäschel, R., Henne, R., Schiller, G. and Greiner, H., Functional layers for the bipolar plates of planar solid oxide fuel cells produced by vacuum plasma spraying. In *Solid Oxide Fuel Cells (SOFC V)*, ed. U. Stimming, S. C. Singhal, H. Tagawa and W. Lehnert. 1997, pp. 1273The Electrochemical Society Proceedings Series, Pennington, NJ, .
3. Heywood, J. B. and Womack, G. J., *Open-cycle MHD power generation*. Pergamon Press, New York, 1969 pp. 568, 609, 613..
4. Mori, M., Yamamoto, T., Itoh, H., Abe, T., Yamamoto, S., Takeda, Y. and Yamamoto, O., Electrical conductivity of alkaline earth metal (Mg, Ca, Sr) doped lanthanum chromites. In *First European SOFC Forum*, ed U. Bossel. Lucerne, Switzerland, 1994, p. 465.
5. Khattak, C. P. and Cox, D. E., Structural studies of $(La,Sr)CrO_3$ system. *Mat. Res. Bull.*, 1977, **12**, 463–471.
6. Mizusaki, J., Yamauchi, S., Fueki, K. and Ishikawa, A., Non-stoichiometry of the perovskite-type oxide $La_{1-x}Sr_xCrO_{3-\delta}$. *Solid State Ionics*, 1984, **12**, 119–124.
7. Anderson, H. U., Kuo, J. H. and Sparlin, D. M. In: *Solid Oxide Fuel Cells (SOFC I)*, ed. S. C. Singhal. The Electrochemical Society Proceedings Series, Pennington, NJ, 1989, p. 111.
8. Flandermeyer, B. K., Nasrallah, M. M., Agarwal, A. K. and Anderson, H. U., Defect structure of Mg-doped $LaCrO_3$: model and thermogravimetric measurements. *J. Am. Ceram. Soc.*, 1984, **67**(3), 195–198.
9. Srilomsak, S., Schilling, D. P. and Anderson, H. U. In *Solid Oxide Fuel Cells (SOFC I)*, ed. S. C. Singhal. The Electrochemical Society Proceedings Series, Pennington, NJ, 1989, p. 129.
10. Schäffer, W. and Schmidberger, R. In *High Tech Ceramics*, ed. P. Vincenzini. Elsevier Science, Amsterdam, Netherlands, 1987, p. 1737.
11. Armstrong, T. R., Stevenson, J. W., Pederson, L. R. and Raney, P. E., Dimensional instability of doped lanthanum chromite. *J. Electrochem. Soc.*, 1996, **143**, 2919–2925.
12. Bausinger, H., Materialeigenschaften von dotierten Perowskiten des Typs $LaCrO_3$, Tübinger Geowissenschaftliche Arbeiten (TGA) Reihe E: Mineralogie, Petrologie und Geochemie; Bd.2000,1; Tübingen. PhD thesis, 2000; Shaker Verlag GmbH, Postfach 1920, 52013 Aachen, Germany.
13. Gut, B., Proceedings of the IEA SOFC Workshop: Sample and Data Bank, Final Report of Activity B3, Annex II: Modelling and Evaluation of Advanced Solid Oxide Fuel Cells, ed. F. W. Poulsen. Riso National Laboratory, Roskilde, Denmark, 1969, p. 12.
14. Milliken, C., Elangovan, S. and Khandar, A., *Proceedings of the 3rd International Symposium on SOFC*. The Electrochemical Society, Pennington, 1993 p. 335.
15. Montross, Ch. Yokokawa, H. and Dokiya, M., *Extended Abstracts of the 60th Meeting of the Electrochemical Society of Japan*, 1993, p. 263.
16. Paulik, S. W., Baskaran, S. and Armstrong, T. R., Mechanical properties of calcium- and strontium-substituted lanthanum chromite. *J. Mater. Sci.*, 1998, **33**, 2397–2404.
17. Kübler, J., *VAMAS Report No.37, ESIS Document D2-99, EMPA*. Swiss Federal Laboratories for Materials Testing and Research, Dübendorf, Switzerland, 1999.
18. Munz, D. and Fett, Th., *Festigkeit Keramischer Werkstoffe*. Springer Verlag, Berlin, 1989.
19. Boroomand, F., Wessel, E., Bausinger, H. and Hilpert, K., Correlation between defect chemistry and expansion during reduction of doped $LaCrO_3$ interconnects for SOFC. *Solid State Ionics*, 2000, **129**, 251–258.

20. Boroomand, F., Wessel, E., Singheiser, L. and Hilpert, K., Oxygen vacancy formation in LaCrO$_3$ base perovskites. In *Solid Oxide Fuel Cells (SOFC-IV)*, ed. S. C. Singhal and M. Dokiya. The Electrochemical Society Softbound Proceedings Series, Pennington, 1999, pp. 666–676 (Proc. Vol. 99-19).

21. Zuev, A., Singheiser, L. and Hilpert, K., Defect structure and isothermal expansion of A-site and B-site substituted lanthanum chromites. *Solid State Ionics*, 2002, **147**, 1–11.

22. Steinbrech, R. W., Toughening mechanism for ceramic materials. *J. Eur. Ceram. Soc.*, 1992, **10**, 131–142.

23. Verwey, E. J. W., Haaijaman, P. W., Romeijn, F. C. and van Oosterhout, G. W., Controlled-valency semiconductors. *Philips Res. Rep.*, 1950, **5**, 173–187.

24. Sehlin, S. R., Anderson, H. U. and Sparlin, D. M., Electrical characterization of the (La,Ca)(Cr,Co)O$_3$ system. *Solid State Ionics*, 1995, **78**, 235–243.

25. Jonker, G. H., Magnetic and semiconductor properties of perovskites containing manganese and cobalt. *J. Appl. Phys.*, 1966, **37**, 1424–1966.

26. Shannon, R. D., Revised effective ionic radii and systematic studies of interatomic distances in halides and chalcogenides. *Acta Cristallogr.*, 1976, **A32**, 751–767.

27. Meschke, F., Kolleck, A. and Schneider, G. A., R-curve behaviour of BaTiO$_3$ due to stress-induced ferroelastic domain switching. *J. Eur. Ceram. Soc.*, 1997, **17**, 1143–1149.

28. Schäufele, A. B. and Härdtl, K. H., Ferroelastic properties of lead zirconate titanate ceramics. *J. Am. Ceram. Soc.*, 1996, **7**, 2637–2640.

29. Montross, Ch., Elastic modulus versus bond length in lanthanum chromite ceramics. *J. Europ. Ceram. Soc.*, 1997, **18**, 353–358.

30. Meschke, F., Raddatz, O., Kolleck, A. and Schneider, G. A., R-curve behaviour and crack-closure stresses in barium titanate and (Mg,Y)-PSZ ceramics. *J. Am. Ceram. Soc.*, 2000, **83**, 353–361.